ScieRxiv

Original Article

SLC9A3R1 functions as an oncogenic driver and a predictor of drug response in hepatocellular carcinoma

Yawen Wu[1†], Guanghao Li[2†], Qiang Li[3], Zhihong Sun[1*], Chengming Sun[1*], Cuicui Wang[1]

[1]The Affiliated Yantai Yuhuangding Hospital of Qingdao University, Yantai 264000, Shandong, China.

[2]Department of Urology, Shandong Cancer Hospital and Institute, Shandong First Medical University and Shandong Academy of Medical Sciences, Jinan 250117, Shandong, China.

[3]Department of Hepatobiliary Tumors, Tianjin Cancer Hospital, Tianjin 300060, China.

Correspondence to: Dr. Zhihong Sun, Prof. Chengming Sun, The Affiliated Yantai Yuhuangding Hospital of Qingdao University, Yantai 264000, Shandong, 264000, China. E-mail: hongzhisun490@163.com; chengmingsun012@163.com

† These authors contributed equally to this work.

Received: 18 May 2026 | Approved: 28 May 2026 | Online: 28 May 2026

Abstract

Aim: Hepatocellular carcinoma (HCC) remains a lethal malignancy with limited therapeutic options and a lack of reliable biomarkers. Solute carrier family 9 member A3 regulator 1 (SLC9A3R1) is implicated in several cancers, yet its comprehensive role and clinical significance in HCC are poorly understood.

Methods: This study integrates multi-omics data, including transcriptomics,

proteomics, copy number variation, methylation, single-cell, and spatial transcriptomics, from various public databases such as TCGA, ICGC, GTEx, CPTAC, HPA, and GEO, and conducts a systematic bioinformatics analysis. Additionally, in the Hep3B cell line, models of SLC9A3R1 overexpression and gene silencing were constructed. Using experiments such as CCK-8, colony formation, Transwell, scratch healing, and flow cytometry, the regulatory effects of this gene on cell proliferation, migration, invasion, apoptosis, and drug sensitivity were validated *in vitro*.

Results: Multi-omics analysis reveals that SLC9A3R1 is significantly overexpressed in HCC due to copy number amplification. This overexpression is closely associated with increased tumor genomic instability, elevated mutation burden, activation of multiple oncogenic pathways, and adverse clinical pathological features. Additionally, SLC9A3R1 influences an immunosuppressive tumor microenvironment marked by lower levels of cytotoxic T cell infiltration. In vitro functional experiments demonstrate that SLC9A3R1 exerts oncogenic effects on proliferation and invasion, and importantly, significantly reduces sensitivity to afatinib—an EGFR/HER2 inhibitor—while inhibiting drug-induced apoptosis. Multi-omics analysis further reveals that SLC9A3R1 expression levels heterogeneously modulate response patterns across 20 chemotherapeutic agents, indicating its role as a broad modulator of drug sensitivity in HCC.

Conclusion: SLC9A3R1 functions as a pivotal oncogenic driver in HCC, enhancing tumor malignancy, shaping an immunosuppressive microenvironment, and facilitating disease progression. Importantly, it acts as a determinant of drug sensitivity, notably conferring reduced sensitivity to afatinib while heterogeneously modulating responses to other therapeutic agents. These findings position SLC9A3R1 not only as a diagnostic and prognostic biomarker and a predictor of immunotherapy response but also as a potential pharmacodynamic indicator for guiding targeted therapy strategies in HCC, thereby offering new molecular targets for precision treatment.

Keywords: SLC9A3R1, hepatocellular carcinoma, multi-omics analysis, tumor microenvironment, immunotherapy, drug sensitivity

INTRODUCTION

Cancer has become a significant challenge in the field of global public health, with mounting death tolls and surging cases, placing a heavy burden on social healthcare systems and patients' families[1]. Among various malignant tumors, Hepatocellular Carcinoma (HCC) is consistently ranks among the top ten in global cancer incidence and mortality rates due to its subtle development, rapid progression, and exceedingly limited treatment outcomes[2]. In our country, influenced by factors such as the high prevalence of hepatitis B virus (HBV) infection and the epidemic of non-alcoholic fatty liver disease, the annual new cases of HCC account for approximately 50% of the global total[3,4]. Despite the continuous development of diagnostic and therapeutic techniques for HCC, surgical resection, transcatheter arterial chemoembolization (TACE), and targeted drugs such as sorafenib and lenvatinib have been widely applied in clinical practice. However, the essential problems in diagnosis and treatment remain unresolved[5,6]. Approximately 60% of patients are identified at an advanced stage, missing the opportunity for curative treatment. Despite surgical intervention, over half of patients experience a relapse within five years, while those with advanced disease have less than a one-in-five chance of surviving that long[7]. Tracing back to the root causes, the lack of molecular markers that reliably reflect HCC progression, prognosis, and treatment response remains the core bottleneck in precision diagnosis and therapy. And with primary or acquired resistance causing over 90% of treatment failures in metastatic cancers, identifying functionally relevant genes and unraveling the key mechanisms behind drug resistance has become an urgent priority in both basic and clinical HCC research.

Solute carrier family 9 member A3 regulator 1 (SLC9A3R1, also known as

NHERF1/EBP50) is a type of scaffold protein characterized by a unique structure. The structure includes two PDZ domains capable of interacting with membrane proteins like G protein-coupled receptors (GPCRs) and receptor tyrosine kinases (RTKs). The carboxy-terminal ERM domain can cross-link with cytoskeletal proteins, thereby precisely regulating the spatiotemporal specificity and intensity of downstream signaling through a mechanism known as “signal complex anchoring”[8-10]. Functionally, SLC9A3R1 serves as a central hub for cellular signal integration, participating not only in the sustaining of epithelial cell polarity and the regulation of membrane receptor transport but also in the integration of critical signaling pathways such as PTEN/PI3K, β-catenin, and Hippo. Dysregulation of its function is closely associated with various human diseases[11,12]. SLC9A3R1 plays a significant role in various cancers. In colorectal cancer, its deletion promotes cancer invasion by facilitating the nuclear accumulation of β-catenin, epithelial-mesenchymal transition (EMT), and tumor budding[13]. In HER2-positive breast cancer, it forms a complex with Erbin and Ezrin to stabilize HER2 signaling on the membrane, thereby promoting tumorigenesis[14]. Additionally, its expression status, in conjunction with tumor-infiltrating lymphocytes, can be used for prognostic stratification in breast cancer patients[15]. It also serves as an efficient detection marker for circulating tumor cells in breast cancer, enhancing diagnostic efficacy[16]. In bladder cancer, it is a differential protein found in urinary exosomes and may serve as a potential diagnostic marker[17]. However, studies on SLC9A3R1 in HCC are still quite limited, and whether—and how—it contributes to drug resistance, let alone its exact role and mechanisms in HCC development and progression, remains largely unclear.

Based on this, the study integrates data from multiple public databases such as The Cancer Genome Atlas (TCGA), the Genotype-Tissue Expression (GTEx), the Clinical Proteomic Tumor Analysis Consortium (CPTAC), and Human Protein Atlas (HPA), along with clinical sample data. Starting from pan-cancer screening, it gradually focuses on HCC. Through multi-dimensional analyses including transcriptomics,

proteomics, epigenomics, single-cell, and spatial transcriptomics, combined with in vitro cell experiments, the study systematically verifies the expression characteristics, regulatory mechanisms, and biological functions of SLC9A3R1. Furthermore, it assesses its clinical value in the diagnosis, prognostic prediction, and guidance of drug sensitivity in HCC, aiming to provide new molecular targets and theoretical basis for the precise diagnosis and treatment of HCC.

METHODS

Multi-omics analysis of cell lines

Immunofluorescence staining images of three tumor cell lines (skin cancer cell A431, glioblastoma cell U-251 MG, and osteosarcoma cell U2OS) were obtained from the HPA database[18] (https://www.proteinatlas.org/) to observe the subcellular localization of the SLC9A3R1 protein. The GSE146773 dataset employed fluorescence activated cell sorting (FACS) to sort a total of 1,152 individual U2OS FUCCI cells, and RNA-Seq was performed on each cell using SMART-seq2. Through single-cell RNA sequencing on the U-2 OS FUCCI cell line, the expression levels of RNA and the phases of the cell cycle were evaluated at an individual cell level. mRNA expression data (nTPM) for SLC9A3R1 in various cancer cell lines were extracted from the HPA database. The protein level data of SLC9A3R1 was sourced from the DepMap database (https://depmap.org/portal/). After screening and extracting quantitative protein level data of SLC9A3R1 across various cancer cell lines including SARC, SKCM, and Bone, the R language ggplot2 package was employed for statistical organization of the data, generating grouped bar charts with error bars. DNA methylation data and genetic variation data were obtained from the Genomics of Drug Sensitivity in Cancer (GDSC) database (https://www.cancerrxgene.org/).

TCGA pan-cancer cohort multi-omics investigation

The molecular characteristic data of the SLC9A3R1 gene were sourced from the TCGA database (https://portal.gdc.cancer.gov/). Using the R package TCGAbiolinks, we

filtered and extracted the mutation profiles (including mutation presence status and mutation frequency) and copy number variation (CNV) profiles of this gene across a range of different cancers, such as Adrenocortical carcinoma (ACC), Bladder urothelial carcinoma (BLCA), and Breast invasive carcinoma (BRCA). The mutation and copy number variation data were then integrated and visualized using the R package ggplot2. Data on gene expression from normal human tissues were sourced from the GTEx database (https://gtexportal.org/). Based on tissue origin, we combined GTEx data with TCGA transcriptome data using the R package ComBat, and then utilized the limma package to identify genes that were differentially expressed when comparing tumor samples to their normal tissue counterparts. Methylation sites in the SLC9A3R1 promoter region were extracted from DNA methylation data, and the methylation status of this gene in tumor versus normal tissues was then compared using a Wilcoxon rank-sum test. The expression patterns of SLC9A3R1 in different cancer types were visualized in multiple dimensions using radar plots. Protein expression data were obtained from CPTAC (https://proteomic.datacommons.cancer.gov/) database. The protein expression differences of SLC9A3R1 between solid tumors and normal tissues were analyzed using the Wilcoxon rank-sum test, which was based on the information regarding sample types.

Diagnostic and prognostic value analysis

Serum exosomal transcriptomic information was obtained from the exosomal database exoRBase (http://www.exorbase.org/) to evaluate the expression levels of SLC9A3R1 in circulating exosomes derived from patients with various forms of cancer, in comparison to healthy controls. Utilizing the expression levels of SLC9A3R1 found in exosomes, we employed the pROC package within R software to generate the receiver operating characteristic (ROC) curve, which helped us assess its diagnostic performance in distinguishing between individuals with cancer and those who are healthy. Based on the SLC9A3R1 expression data and objective response rate (ORR) data from clinical records in the TCGA database, a scatterplot with fitted line was

generated using the ggplot2 package in R language. The scatter points represent different cancer types, with a blue fitted line illustrating their trend of variation. The gray shaded area indicates the 95% confidence interval. Pearson correlation coefficient (r) and corresponding *P*-value were calculated and annotated to quantify the association between SLC9A3R1 expression levels and ORR[19]. Drawing upon molecular typing data from the TCGA pan-cancer cohort, the expression differences of SLC9A3R1 across different molecular subtypes were evaluated through the Wilcoxon rank-sum test. Clinical staging information from TCGA was used to explore the link between SLC9A3R1 levels and tumor stages (I-IV). Each group must contain at least 5 samples. Trend analysis is performed using the Mann-Kendall trend test. Furthermore, a comparison of SLC9A3R1 expression was made based on histological grading data, distinguishing between high-grade (G3 & G4) and low-grade (G1 & G2) groups, covering cancer types such as Cervical squamous cell carcinoma and endocervical adenocarcinoma (CESC), Esophageal carcinoma (ESCA), Head and neck squamous cell carcinoma (HNSC), Brain lower grade glioma (LGG), Liver hepatocellular carcinoma (LIHC), Ovarian serous cystadenocarcinoma (OV), Stomach adenocarcinoma (STAD), Uterine corpus endometrial carcinoma (UCEC). Survival endpoint information, which included metrics like overall survival (OS), disease-specific survival (DFS), disease-free interval (DFI), and progression-free interval (PFI), was retrieved from the TCGA database. The prognostic value of SLC9A3R1 was established via univariate Cox and Kaplan-Meier survival analyses.

Analysis of SLC9A3R1 expression patterns and clinical prognosis in a multicenter dataset of HCC

We first retrieved a series of HCC-related datasets including GSE10143, GSE105130, GSE12941, GSE135631, GSE147888, GSE16928, GSE184733, GSE19665, GSE207435, GSE14846, GSE25097, GSE36376, GSE39791, GSE45436, GSE54238, GSE57957, GSE84005, GSE87410, GSE87630, GSE45050, GSE89377, GSE114564, GSE76427, GSE144269, and GSE116174 from the Gene Expression Omnibus (GEO,

https://www.ncbi.nlm.nih.gov/geo/), while obtaining HCC cohort gene expression data from the International Cancer Genome Consortium database (ICGC, https://dcc.icgc.org/). Subsequently, all included samples were grouped according to tumor type and clinical stage. Finally, we compared SLC9A3R1 gene expression variations among various cohorts by employing both the Wilcoxon rank-sum test and the Kruskal-Wallis rank-sum test methods. Images from the HPA database were collected for normal liver tissue as well as for tumor tissue through immunohistochemical analysis. The antibody used was an anti-SLC9A3R1 primary antibody (HPA 009672, CAB001962). Transcriptional data from three liver cancer-related datasets, GSE10141, GSE76427, and GSE144269, were obtained from the GEO. Concurrently, transcriptional data and survival follow-up information from the clinical data of the ICGC-LIRI-JP liver cancer cohort were retrieved from the ICGC. This research employed the Kaplan-Meier survival analysis strategy, utilizing the R language's survival package for data analysis. The samples from each cohort were classified into groups of high and low expression according to the median expression level of the SLC9A3R1 gene. Subsequently, the Log-rank test was administered using the survfit function, which allowed us to determine if the variations in survival rates between the two groups were statistically noteworthy.

Spatial transcriptomics analysis.

To intuitively visualize the expression distribution patterns of target genes across different microregions of tissues, this study conducted spatial transcriptomic analysis of target tissue sections utilizing the SpatialTME database (https://www.spatialtme.yelab.site/#!/). The analytical workflow proceeds as follows. First, the raw spatial transcriptomic expression count data undergoes normalization via the NormalizeData function to eliminate technical variations between samples, ensuring the accuracy of subsequent analyses. Next, the Seurat package's SpatialFeaturePlot function is employed to generate spatial dot plots of gene expression (with individual dot diameters of approximately 55 μm, where color intensity visually

represents expression levels), while its SpatialPlot concurrently shows dominant cell types per microregion alongside their spatial arrangement. Consequently, Spearman correlation analysis quantifies the relationships between cellular abundances within microregions, alongside the relationship between cellular abundances and target gene expression levels, with multidimensional visualization of correlation results achieved using the linkET package. Finally, the Cottrazm package integrates cluster analysis with high CNV signatures of tumor cells to identify tumor core regions, extrapolates adjacent microregions based on a hexagonal system, and calculates Uniform Manifold Approximation and Projection (UMAP) distances to precisely delineate tumor boundary regions. Concurrently, the fromto package's dplot5 function visualizes average target gene expression across different regions, while the R language wilcox.test function performs Wilcoxon rank-sum tests to evaluate expression differences of target genes between regions.

Single-cell analysis of SLC9A3R1 in HCC

This study obtained three independent HCC single-cell RNA sequencing datasets (GSE125449, GSE146115, GSE166635) from the GEO database for analysis of the SLC9A3R1 gene. First, the technique known as Uniform Manifold Approximation and Projection (UMAP) was utilized to reduce the dimensionality of the single-cell expression data, transposing the high-dimensional dataset into a two-dimensional representation. Cell clustering was achieved based on the similarity of cellular expression profiles, with distinct cell types color-coded accordingly. Additionally, the Nebulosa package was utilized to integrate intercellular similarity through weighted kernel density estimation and recover lost gene signals, thereby optimizing the visualization of SLC9A3R1-related single-cell data. To elucidate the varying expression of SLC9A3R1 among different cell types, the expression levels of this gene were initially measured in each cell type. Subsequently, the Kruskal-Wallis rank sum test was employed to evaluate the statistical significance of differences in expression across groups. Additionally, all cell subpopulations were grouped based on the

positive/negative status of SLC9A3R1 expression, and the proportions of each cell subpopulation in the two groups were calculated to analyze the cell-type-specific expression contribution characteristics of this gene. The analysis of intercellular interactions was conducted using the CellPhoneDB ligand-receptor interaction database. First, fibroblast, endothelial cells, $CD8^{+}$T cells, hepatic progenitor cells, M1-type macrophages, plasma cells, and other cell populations were annotated based on specific marker genes, and malignant cells were further classified into SLC9A3R1+ and SLC9A3R1- subtypes according to SLC9A3R1 expression levels. Subsequently, the total number of significant ligand-receptor interaction pairs between different cell types was counted to characterize interaction quantity, while interaction strength scores were calculated based on the built-in algorithm (weighted product of ligand-receptor expression levels). Additionally, by combining weighted quantification of ligand/receptor expression levels and pathway enrichment, the signal output strength (as ligand providers) and signal input strength (as receptor receivers) of each cell type were determined. Finally, the R package pheatmap was used to generate heatmaps, visually displaying differences in signaling strength across various pathways among different cell types.

Analysis of copy number variation, mutation, and immune characteristics of SLC9A3R1 in TCGA-LIHC

To comprehensively investigate the role of SLC9A3R1 in HCC, this study utilized public data from TCGA-LIHC. CNV data were processed through the TCGA FIREHOSE analysis pipeline using the GISTIC2 algorithm. The GISTIC scores were visualized in a bar plot, with blue and yellow representing copy number amplification and deletion, respectively. Patients were categorized into four quartiles (Q1-Q4) based on SLC9A3R1 expression levels. Q1 represented the top 25% of patients exhibiting the highest expression, while Q4 encompassed the bottom 25% with the lowest expression(20). Genomic instability was quantified using the fraction of genome altered (FGA), fraction of genome gained (FGG), and fraction of genome lost (FGL). Samples

were categorized into high and low SLC9A3R1 expression groups based on the median expression level. Gene expression heatmaps were created with the pheatmap package in R. The study employed scatter plots and Spearman's rank correlation to examine the relationship between SLC9A3R1 copy number variations and corresponding mRNA expression levels. The Kruskal-Wallis test was applied to compare variations in gene expression across the four CNV subtypes. The study processed single nucleotide variation (SNV) data from the TCGA-LIHC cohort to calculate mutation frequencies and utilized the maftools package to generate mutation profiles. Tumor mutation burden (TMB) and neoantigen data were sourced from previous studies[20], with intergroup comparisons performed using Wilcoxon rank-sum tests. The study analyzed the distribution differences of molecular subtypes between SLC9A3R1 high- and low-expression groups through chi-square tests, with molecular subtype annotation information extracted from published literature[20]. In the analysis of immune microenvironment, the Tumor Immunophenotype (TIP) database was utilized to evaluate the anti-tumor immune response levels across seven steps of the cancer-immunity cycle. Spearman’s rank correlation test was utilized to explore the link between SLC9A3R1 expression levels and TIP ratings, with visualization accomplished using the linkET package. Immune infiltration data were obtained from the TIMER 3.0 database, and Spearman correlation coefficients between immune cell types and gene expression were presented in heatmaps. Immune regulatory genes related to antigen presentation and chemokine signaling pathways were sourced from the TISIDB database. Statistical processing and data visualization were carried out using R.

Analysis of tumor immune microenvironment and methods for treatment response evaluation

The Tertiary Lymphoid Structure (TLS) scoring data was sourced from the IMPACT online tool (https://impact.brbiotech.com/), with its relationship to SLC9A3R1 expression analyzed through scatter plots and box plots. Statistical significance was

assessed using Spearman correlation analysis and Wilcoxon rank-sum test. Tumor immune escape potential was evaluated via the TIDE database (http://tide.dfci.harvard.edu/), where expression data across different treatment stages was standardized using Z-scores. Intergroup difference testing was performed using the `wilcox.test` function in R language. Analysis of T-cell dysfunction and exclusion characteristics was conducted based on the TIMER3.0 platform (https://compbio.cn/timer3/). Spearman correlations between SLC9A3R1 expression and these two features were calculated separately and visualized. For chemotherapeutic response assessment, the pRRophetic software package was employed to predict clinical chemotherapy responses. This was combined with small-molecule drug dose-response data from the Cancer Therapeutics Response Portal (CTRP, https://portals.broadinstitute.org/ctrp/) to screen the top 20 drugs ranked by sensitivity and resistance. To mitigate interference from extreme values, the expression data and drug sensitivity AUC values were first standardized using the `scale` function for Z-score normalization, followed by calculating Spearman correlation between them using the 'cor.test' function. The heterogeneity of SLC9A3R1's drug sensitivity modulation patterns across different cohorts was ultimately visualized through heatmaps. Meanwhile, for representative drugs such as afatinib and SU11274, the association between SLC9A3R1 expression and their half-maximal inhibitory concentration (IC50) was analyzed, employing non-parametric tests and correlation analysis methods to complete statistical inference and graphical presentation.

Analytical methods for associating carcinogenic signaling pathways with phenotypes

The assessment of oncogenic signaling pathway activity was conducted in the TCGA-LIHC cohort using the IMPACT online tool (https://impact.brbiotech.com/) to analyze eight classical pathways. The z-scores for the combined gene sets of pathways were computed utilizing the z-score functionality within the GSVA package, and pathway activity scores were generated after standardization with the scale function.

Analysis of tumor malignant phenotypes utilized ten functional state gene sets provided by the CancerSEA database (http://biocc.hrbmu.edu.cn/CancerSEA/), with standardized scores similarly computed through gene set variation analysis (GSVA). The association between SLC9A3R1 expression and various scores was evaluated using Pearson correlation analysis. For the analysis of differential expression, we divided our samples into high-expression and low-expression cohorts based on median expression levels, then employed the limma package to make comparisons between these groups (screening criteria: |logFC|>2, FDR<0.05). Genes that were expressed at varying levels were later analyzed for enrichment in the Kyoto Encyclopedia of Genes and Genomes (KEGG) via the clusterProfiler package, and the significance of each term was determined through a hypergeometric test (FDR-adjusted threshold $p \leq 0.05$). Gene set enrichment analysis (GSEA) analysis based on Hallmark gene sets was conducted using the same package, with normalized enrichment scores (NES) calculated and multiple hypothesis correction applied.

Cell proliferation and migration *in vitro*

In vitro proliferation assay: Experimental and control group Hep 3B cells were plated in 96-well dishes and cultured at 37 °C under a 5% CO_2 environment. After incubation, detection reagent (Sparkjade, China) was added and incubated for 1 h. Optical density value was measured at 450nm wavelength by microplate reader to evaluate cell proliferation ability.

Clone formation experiment: The cells of each group were inoculated into 6-well plate at appropriate density, and after 14 days of culture, they were treated with 4% paraformaldehyde and stained using 0.1% crystal violet, after which the clone count was determined.

Cell migration assay: In order to inhibit cell proliferation, Hep 3B cells were incubated in serum-free medium. Cells from the experimental and control groups were seeded in

the upper chamber of a 0.8 μm transwell chamber (Corning), and 750μL of medium containing 10% FBS was added to the lower chamber, and incubated at 37 ℃ and 5% CO_2 for 24 h. After incubation, non-migrating cells on the upper surface of the membrane were gently removed with cotton swabs, images were captured by an inverted microscope, and migrating cells were counted by ImageJ software.

Cell invasion assay: The experimental procedure was identical to that of migration assay, except that the bottom membrane of the upper chamber was pre-coated with 25% Corning, and the invading cells were subsequently observed and counted by the same method.

Cell wound healing assay: Cells were seeded in 6-well plates and incubated at 37 °C until reaching 95% density. A wound was created in the cell monolayer using a sterile 200 μL pipette tip. Cell migration was observed and images were captured at 0 and 24 h under a microscope, and the migration distance was analyzed using ImageJ software.

Analysis of drug sensitivity and apoptosis: To evaluate the role of SLC9A3R1 in the response to afatinib, cell viability was assessed using the CCK-8 assay as described above after treatment with varying concentrations of afatinib. For apoptosis analysis, cells from the SLC9A3R1 overexpression and vector control groups were treated with afatinib (6 μM). The proportion of early and late apoptotic cells was then detected and analyzed by flow cytometry.

Statistical analysis

Group comparisons were conducted using either parametric or non-parametric tests, based on the distribution characteristics of the data. For continuous variables displaying a normal distribution, a *t*-test was utilized, on the other hand, for continuous variables not following a normal distribution, the Wilcoxon rank-sum test or the Kruskal-Wallis test was conducted. Correlation analyses were conducted using methods suited for the

type of variables involved. Pearson correlation analysis was utilized for examining relationships between continuous variables. The effectiveness of diagnostics was evaluated through the analysis of ROC curves. To assess survival, the Kaplan-Meier technique was employed to chart survival curves, while the Log-rank test was used to identify discrepancies across the different cohorts. Cox proportional hazards regression models, both univariate and multivariate, were applied to evaluate the influence of various factors on prognosis, presenting the findings as hazard ratios accompanied by their respective 95% confidence intervals. In order to address the issue of false discovery rate, we applied the Benjamini-Hochberg correction technique for handle multiple testing. We performed all statistical analyses using two-tailed tests and set our significance cutoff at $P < 0.05$.

RESULTS

Multi-omics profiling of SLC9A3R1 highlights its pan-cancer oncogenic features

To elucidate the subcellular distribution characteristics, cell cycle-dependent expression patterns, and pan-cancer molecular features of SLC9A3R1, this research carried out a systematic investigation by combining multi-omics technologies and public database resources. Through the analysis of immunofluorescence staining data (including skin cancer cell line A431, glioblastoma cell line U-251 MG, and osteosarcoma cell line U2OS) in HPA database, it was found that this protein exhibits a dual localization pattern at the cell membrane and centrosomal satellite regions in all three tumor cell lines, while also showing spatial co-localization with the endoplasmic reticulum, microtubule network, and nuclear structures [Figure 1A]. Further analysis of cell cycle transcriptomic data (GSE146773) for temporal expression analysis revealed that in U2OS cells, the mRNA abundance of SLC9A3R1 exhibited distinct periodic fluctuations, with significantly higher expression in the G1 phase compared to the S and G2/M phases [Figure 1B]. To explore the expression profile of SLC9A3R1 in neoplastic cells, we performed an extensive transcriptomic study via the HPA database. The results shown in Figure 1C indicate that the levels of mRNA expression for

SLC9A3R1 differ notably across various cancer cell lines: the expression level of this gene is highest in breast cancer cells, reaching 462.6 nTPM, followed by multiple myeloma (MM) (214.8 nTPM) and liver cancer cells (207.4 nTPM). Conversely, the three cancer cell lines with the lowest expression are adrenocortical carcinoma and neuroblastoma (both with expression levels of 30.6 nTPM), as well as rhabdomyosarcoma (35.4 nTPM). The DepMap database demonstrates the protein levels of this gene across various cancer types, where significant differences in protein levels are evident. For instance, cancers such as MM, RCC, BRCA, and LIHC exhibit relatively high protein levels, which is consistent with the cellular expression patterns [Figure 1D]. Additionally, the epigenetic analysis using the GDSC database revealed significant cancer type-specific DNA methylation modifications in the SLC9A3R1 gene. Specifically, hypermethylation was observed in cancers such as acute lymphoblastic leukemia (ALL), lymphoid malignancies, and RCC, whereas relatively lower methylation levels were found in BRCA, small cell lung cancer (SCLC), and colorectal cancer (CRC) [Figure 1E]. Analysis of the genetic variation characteristics of the SLC9A3R1 gene across different cancer types reveals that, at the copy number level, SLC9A3R1 exhibits a high frequency of alterations in cells from various cancers, including neuroblastoma (NB), prostate cancer (PRCA), head and neck cancer (HNC), BRCA, and HCC. Notably, neuroblastoma shows the highest amplification frequency, while prostate cancer exhibits the highest deletion frequency [Figure 1F]. Through systematic multi-angle analysis, this research found that this protein not only possesses cycle-specific regulatory capabilities but also exhibits unique epigenetic modification characteristics and high-frequency mutation phenomena, indicating its potential significant role in the development and advancement of various cancers.

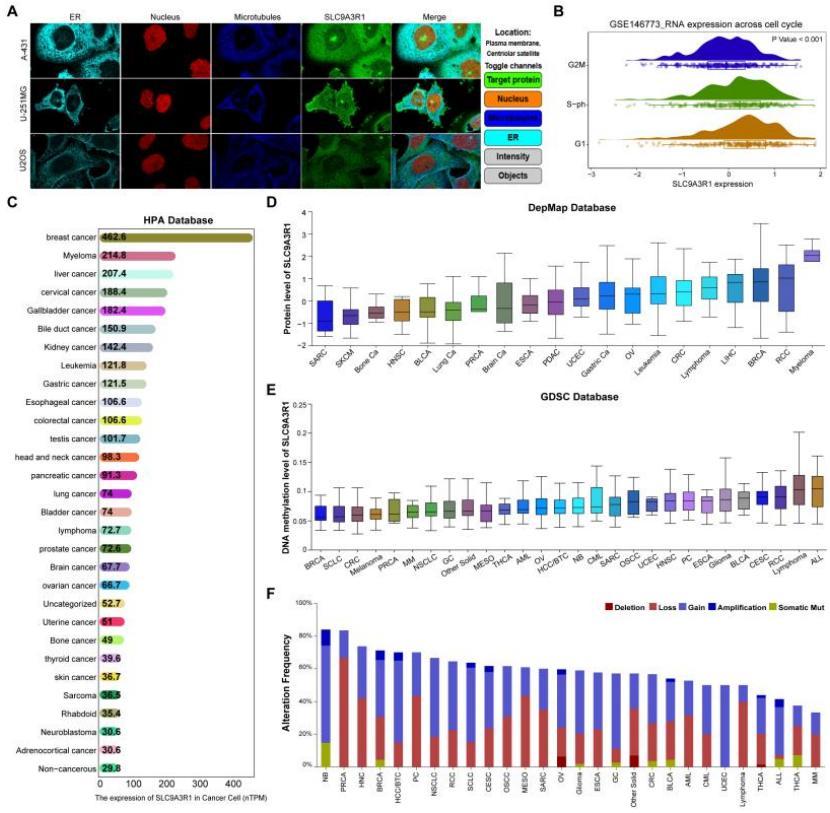

Figure 1. Multi-omics profiling of SLC9A3R1 highlights its pan-cancer oncogenic features. (A). Representative immunofluorescence images illustrate the subcellular localization of SLC9A3R1 (green) in A431, U-251 MG, and U2OS cell lines, as sourced from the HPA database. Cell structures are counterstained with endoplasmic reticulum (ER, yellow), microtubules (red), and nuclei (blue). Scale bar: 10 micrometers; (B). mRNA expression levels of SLC9A3R1 in U2OS cells at different cell cycle stages based on transcriptomic data (GSE146773); (C). mRNA expression levels of SLC9A3R1 (nTPM) in various cancer cell lines from the HPA database; (D). The DepMap database demonstrates the protein levels of SLC9A3R1 across various cancer types; (E). DNA methylation levels (Beta values) of SLC9A3R1 in different cancer types from the GDSC database; (F). Genetic alteration profiles of SLC9A3R1 across various cancer types from GDSC, showing the frequency of mutations, amplifications, and deletions.

SLC9A3R1 is upregulated in pan-cancer tissues and is accompanied by low methylation of its promoter

After clarifying the basic characteristics of SLC9A3R1 at the cell line level, we further utilized clinical tissue databases such as TCGA, GTEx, and CPTAC to systematically validate its expression and regulatory patterns at the human tissue level. Figure 2A presents a comprehensive pan-cancer map that illustrates the widespread dysregulation of SLC9A3R1 across various cancer types. This dysregulation includes transcript upregulation, copy number variations, and epigenetic alterations. Notably, although the mutation frequency of SLC9A3R1 remains generally low across malignancies, it exhibits variable degrees of copy number amplification and deletion among various cancer types. For instance, kidney renal papillary cell carcinoma (KIRP) demonstrates the highest frequency of SLC9A3R1 copy number amplification, while kidney chromophobe (KICH) shows the highest frequency of copy number deletion. To elucidate the processes driving alterations in the expression of SLC9A3R1, we performed an in-depth analysis of the epigenetic data from the TCGA pan-cancer exhibited a hypomethylated status in various malignant tumors, including BLCA, BRCA, CESC, colon adenocarcinoma (COAD), kidney renal clear cell carcinoma (KIRC), KIRP, LIHC, lung squamous cell carcinoma (LUSC), prostate adenocarcinoma (PRAD), and rectum adenocarcinoma (READ) [Figure 2B]. We integrated transcriptomic data from TCGA and GTEx and found that SLC9A3R1 mRNA is significantly upregulated in most of the analyzed cancer types. This expression profile remains stable across both male and female patient populations, demonstrating its reliability across populations [Figure 2C]. The radar chart in Figure 2D visualizes the universally elevated expression pattern of SLC9A3R1 across various cancers. Finally, we confirmed the above findings at the protein level. Analysis of proteomic data from the CPTAC database showed that SLC9A3R1 protein levels are markedly elevated in several solid tumors, such as BRCA and LIHC, in comparison to normal tissue [Figure 2E]. In conclusion, the gathered data collectively indicate that SLC9A3R1 is a consistently upregulated molecule in pan-cancer, with its increased expression likely linked to a low methylation profile in the promoter region.

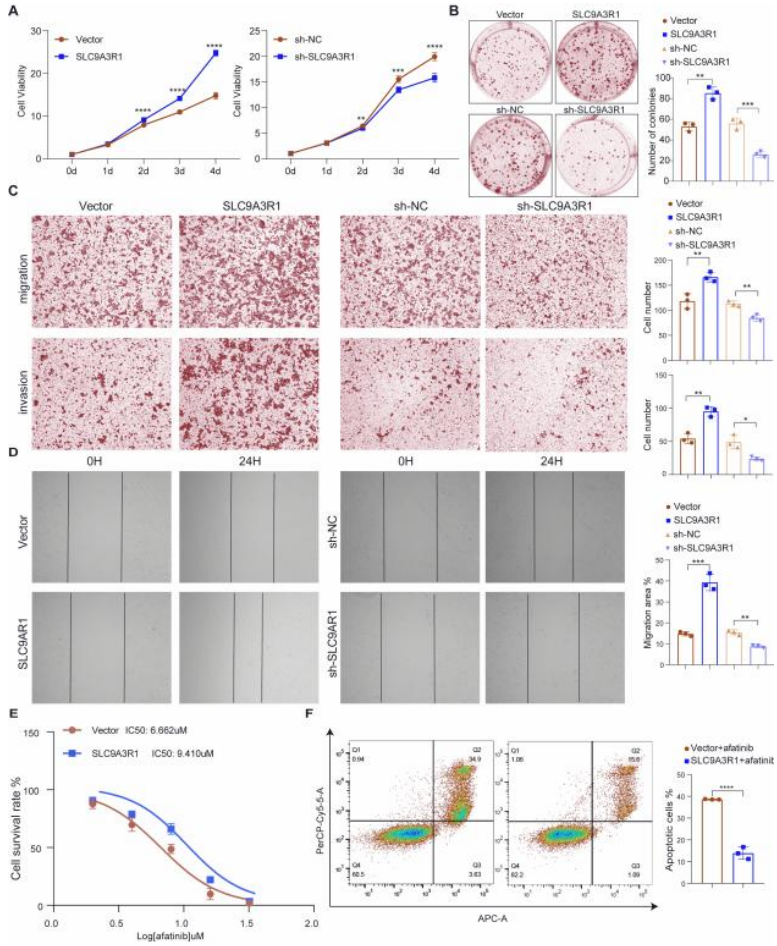

Figure 2. SLC9A3R1 is upregulated in pan-cancer tissues and is accompanied by low methylation of its promoter. (A). A comprehensive pan-cancer atlas of SLC9A3R1 alterations across multiple cancer types from the integrated clinical organization database reveals transcriptional upregulation, copy number variations, and epigenetic modifications; (B). Comparison of DNA methylation levels (Beta values) in the SLC9A3R1 promoter region between tumor tissues and corresponding normal tissues from the TCGA database; (C). Comparison of SLC9A3R1 mRNA expression levels (nTPM) across various cancer types with normal tissues, stratified by male and female patient cohorts, using integrated data from TCGA and GTEx; (D). Radar chart visualizing the multidimensional expression patterns of SLC9A3R1 in different cancer types; (E). Comparison of SLC9A3R1 protein expression levels in solid tumors (BRCA, COAD, OV) versus normal tissues from the CPTAC proteomics database.

The potential and prognostic value of SLC9A3R1 as a cancer diagnostic marker

Given the stable upregulation of SLC9A3R1 expression across various cancer tissues and its regulatory mechanisms related to epigenetic modifications, we further expanded our research scope to investigate its expression in clinically accessible serum exosomes. An extensive examination of the exoRBase database was carried out by us, and the findings are illustrated in Figure 3A. SLC9A3R1 was detected in circulating exosomes from patients with various malignancies, including BRCA, CRC, HCC, KIRC, melanoma (ML), non-small cell lung cancer (NSCLC), OV, and SCLC, with expression levels significantly higher than those of healthy controls. Subsequently, we further assessed the diagnostic efficacy of exosomal SLC9A3R1. The ROC curve analysis presented in Figure 3B indicates that exosomal SLC9A3R1 possesses exceptional ability to differentiate cancer patients from healthy individuals, suggesting it holds promise as a diagnostic marker with potential utility in the supplementary diagnosis of cancer. We also investigated the link between the levels of its expression and the results of treatment. Across distinct malignancies, a significant inverse relationship emerged between SLC9A3R1 levels and the ORR (Pearson r = -0.281, P = 0.032). This finding implies that cancer patients exhibiting high levels of SLC9A3R1 may experience reduced treatment effectiveness [Figure 3C]. From the viewpoint of tumor heterogeneity, elevated levels of SLC9A3R1 are strongly linked to more aggressive biological subtypes [Figure 3D]. Examination of SLC9A3R1 expression patterns across different cancer stages (from I to IV) suggests a significant association with advancing tumor stage. Across different types of cancer, including testicular germ cell tumor (TGCT), LIHC, KIRC, and CESC, a clear increase in SLC9A3R1 expression was noted as the tumor stage advanced [Figure 3E]. In addition, we conducted an analysis related to histological grading in the TCGA pan-cancer cohort. The results indicated that in LIHC and OV, the expression level of SLC9A3R1 in the high-grade groups (G3, G4) was markedly elevated compared to that in the low-grade groups (G1, G2). Conversely, in CESC, ESCA, HNSC, LGG, STAD, and UCEC, a markedly lower expression of this gene was observed in the high-grade groups relative to their low-grade counterparts. This finding reflects the cancer type-specific expression pattern of SLC9A3R1 at the

pathological level, suggesting that its association with malignant tumor phenotypes may vary depending on the type of cancer [Figure 3F]. Ultimately, through the integration of the prognostic implications of SLC9A3R1 across different cancers, it became evident that this gene acts as a risk factor correlated with unfavorable prognosis in cancers LAML and LIHC, while also having a significant effect on patient survival outcomes in cancers such as pheochromocytoma and paraganglioma (PCPG) and prostate adenocarcinoma (PRAD) [Figure 3G]. This systematic analysis suggests that SLC9A3R1 could function as a prognostic biomarker across multiple cancer types, offering multidimensional support for clinical prognosis evaluation.

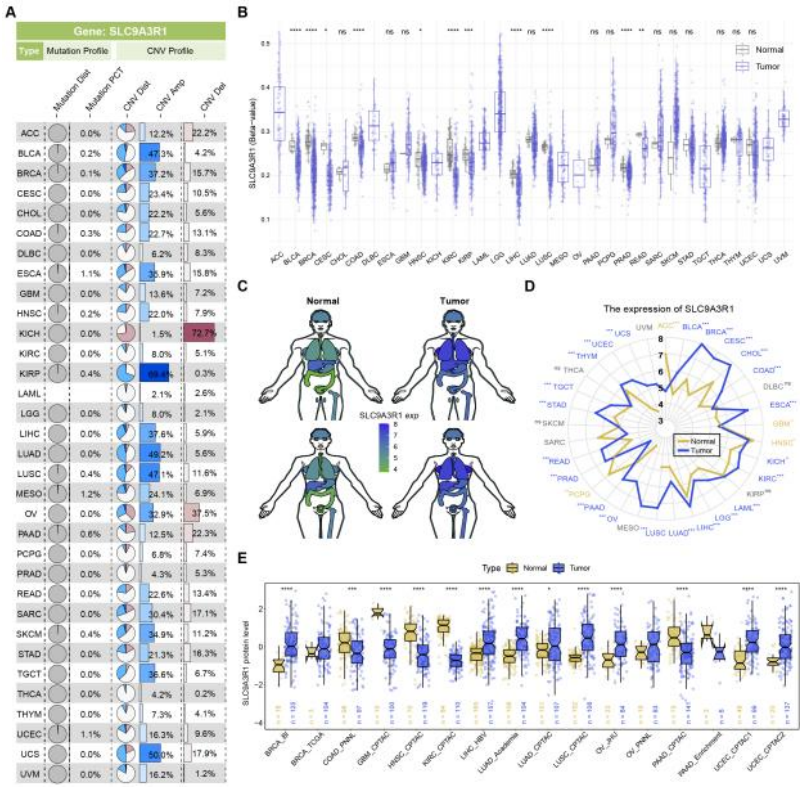

Figure 3. The Potential and Prognostic Value of SLC9A3R1 as a Cancer Diagnostic Marker. (A). Detection of SLC9A3R1 in circulating serum exosomes of various cancer patients and healthy controls using the exoRBase database; (B). Assessing exosomal SLC9A3R1 efficacy in differentiating cancer cases from healthy controls via ROC curve analysis; (C). Correlation analysis between SLC9A3R1 expression levels and objective response rate (ORR) in multiple cancer types; (D). Analysis of SLC9A3R1 expression levels across different molecular subtypes of various cancers in the TCGA

database; (E). Patterns of SLC9A3R1 expression across tumor stages (I-IV) in multiple cancer types within the TCGA database; (F). Expression levels of SLC9A3R1 across various histological grades (G1&G2 *vs.* G3&G4) in different cancers within the TCGA pan-cancer cohort; (G). Heatmap summarizing the prognostic significance of SLC9A3R1 in different cancer types, including hazard ratios for OS, DSS, DFI, and PFI.

A multimodal association analysis of SLC9A3R1 expression profiles with clinical staging and prognosis in HCC

Building on the results showing increased expression of SLC9A3R1 and its clinical relevance uncovered in the initial pan-cancer analysis, this research aims at a multi-faceted validation specifically targeting HCC. The analysis of multiple independent HCC datasets shows [Figure 4A] that a notable increase in the mRNA expression levels of this gene within tumor tissues in comparison to adjacent non-tumor tissues, with a consistent and highly significant upregulation trend observed across 20 cohorts. Furthermore, the protein-level enhancement was confirmed via immunohistochemistry (IHC) data sourced from the HPA database, which demonstrated markedly intensified SLC9A3R1 immunostaining in HCC tissues compared to that in the adjacent liver parenchyma [Figure 4B]. To further explore the dynamic expression pattern of SLC9A3R1 during liver cancer progression, we integrated and examined multiple transcriptomic datasets covering different stages of liver disease. The comprehensive results indicate a robust connection between the expression levels of SLC9A3R1 and the advancement of liver diseases leading to HCC, it shows a significant upregulation trend in the sequential evolution from chronic hepatitis and cirrhosis to HCC, and its expression in advanced HCC is significantly higher than in early stages (GSE45050, GSE54238, GSE89377, GSE114564) [Figure 4C-F]. We conducted an analysis to explore the relationship between SLC9A3R1 expression levels and both clinical staging and patient outcomes in liver cancer. Figure 4G-J demonstrate that in various independent datasets, including GSE76427, GSE144269, GSE116174,

and ICGC-LIRI-JP, patients with advanced liver cancer (stages III-IV) exhibited considerably higher levels of SLC9A3R1 compared to those with early-stage disease (stages I-II). Moreover, Figure 4K-N depict that an overall survival analysis performed across four distinct liver cancer cohorts (GSE10141, GSE76427, GSE144269, and ICGC-LIRI) showed that individuals having elevated SLC9A3R1 levels experienced significantly reduced OS when compared to those with low levels. Overall, these findings collectively indicate that SLC9A3R1 is not only upregulated as liver cancer progresses but also closely linked with negative clinical outcomes.

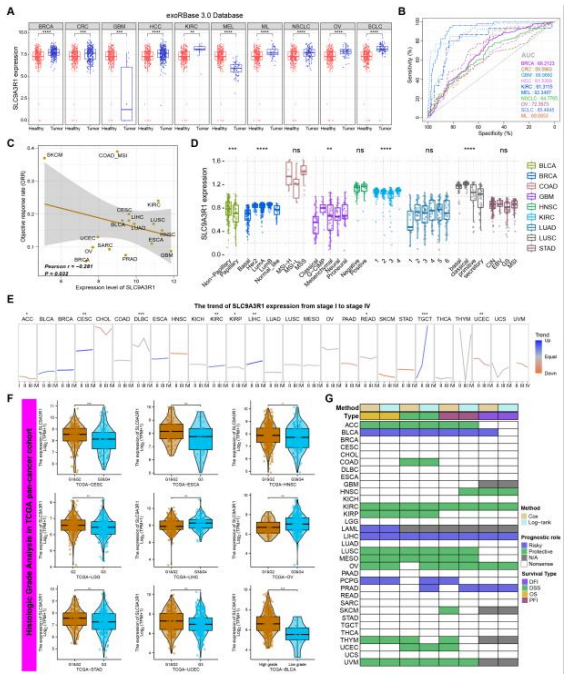

Figure 4. A multimodal association analysis of SLC9A3R1 expression profiles with clinical staging and prognosis in HCC. (A).SLC9A3R1 mRNA levels in HCC tumors versus adjacent normal tissues from multiple datasets; (B). Immunohistochemical staining of SLC9A3R1 protein in normal liver tissues and HCC specimens was obtained from the HPA database; (C-F); Dynamic expression patterns of SLC9A3R1 during the progression of liver disease from chronic hepatitis and cirrhosis to early and advanced HCC in multiple transcriptomic datasets (GSE45050, GSE54238, GSE89377 and GSE114564); (G-J). Expression levels of SLC9A3R1 in early (stages I-II) and advanced (stages III-IV) HCC patients across multiple independent cohorts (GSE76427,

GSE144269, GSE116174, and ICGC-LIRI-JP); (K-N). Kaplan-Meier overall survival analysis of HCC patients stratified by SLC9A3R1 expression levels in four independent cohorts (GSE10141, GSE76427, GSE144269, ICGC-LIRI).

Through a systematic analysis of six HCC tissue samples utilizing spatial transcriptomics[21,22], this study elucidated the significant spatial expression heterogeneity of SLC9A3R1 within HCC tissues. SLC9A3R1 showed significantly higher expression levels in the tumor core (Mal) when compared to the levels found in the tumor periphery (Body) and in the surrounding normal tissue (nMal), with a pronounced enrichment in malignant regions. Subsequent spatial co-localization analysis revealed extensive overlap between regions of high SLC9A3R1 expression and the presence of tumor cells, macrophages, and endothelial cells. Furthermore, SLC9A3R1 expression exhibited a gradient distribution, diminishing progressively from the tumor core to normal tissue [Figure 5]. These findings establish SLC9A3R1 as a spatially regulated, microenvironment-associated key molecule in HCC, providing a basis for its potential as a therapeutic target for tumor core-targeted therapy.

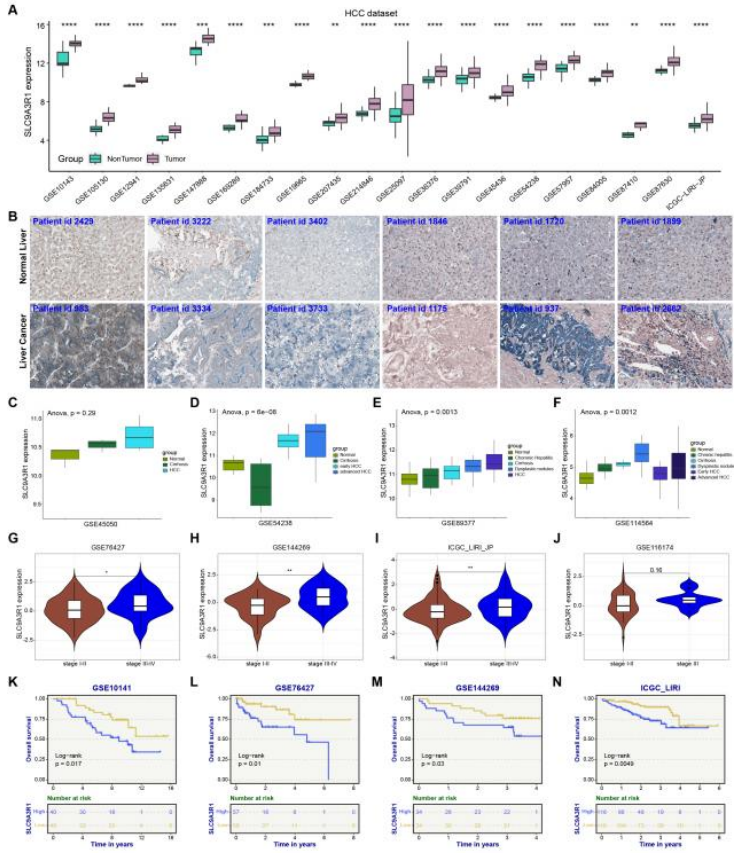

Figure 5. Spatial transcriptomic analysis of SLC9A3R1 in HCC. H&E staining of HCC tissue section. Identification of malignant and non-malignant regions in HCC tissue. Cell type composition analysis at spatial transcriptome resolution. Correlation analysis between SLC9A3R1 expression and TME cell composition. Comparison of SLC9A3R1 expression levels between malignant and non-malignant regions.

SLC9A3R1+ malignant cells act as signaling hubs coordinating the microenvironment through the VEGF pathway

To further clarify the regulatory function of SLC9A3R1 within the tumor microenvironment (TME), we analyzed its expression status in relation to the proportions of immune cells, malignant cells, and stromal cell subpopulations, as well as intercellular signaling interactions within tumor tissues. We integrated analyses from three independent single-cell RNA sequencing datasets of liver cancer (GSE125449, GSE146115, GSE166635). UMAP dimensionality reduction clustering deconstructed the TME into core components including malignant tumor cells, $CD8^+$ T cells ,

macrophages (M1), fibroblasts, and endothelial cells [Figures 6A-C]. Expression analysis indicated that the expression of SLC9A3R1 exhibited a high degree of cell specificity, its mRNA abundance in malignant tumor cells was significantly higher than that in various immune and stromal cells, and this trend was highly consistent across multiple datasets, confirming that SLC9A3R1 is a molecule predominantly associated with malignant cells. Intercellular communication analysis based on CellChat further revealed the central position of SLC9A3R1+ malignant cells within the TME signaling network. This cell type exhibited the highest number of interaction connections with other cell types [Figure 6D], and the overall communication strength was significantly greater than that of other cells [Figure 6E]. Signal role analysis demonstrated that SLC9A3R1+ malignant cells displayed a very strong capacity for both outgoing and incoming signaling, establishing their role as dominant regulators within the interaction network [Figure 6F]. To further identify the specific signaling pathways dominated by SLC9A3R1+ malignant cells, we conducted a systematic analysis of ligand-receptor interactions. The results indicated that among the numerous signaling pathways led by SLC9A3R1+ malignant cells, the VEGF signaling pathway was particularly prominent. The number of interactions and the functional importance score of this pathway in SLC9A3R1+ cells were notably greater than those in SLC9A3R1- malignant cells [Figure 6G]. A deeper analysis of the intercellular communication network within the VEGF pathway revealed that SLC9A3R1+ malignant cells primarily act as signal senders, establishing close VEGF signaling connections with stromal components such as fibroblasts and endothelial cells [Figure 6H]. This result suggests that SLC9A3R1+ malignant cells may selectively enhance VEGF signaling to promote stromal remodeling and angiogenesis, thereby collaboratively facilitating tumor progression. In summary, this study confirms at the single-cell level that SLC9A3R1 is specifically highly expressed in malignant tumor cells in liver cancer and serves as a core hub in the TME signaling network. By significantly reinforcing key pathways such as VEGF, it actively regulates the stromal and immune microenvironment.

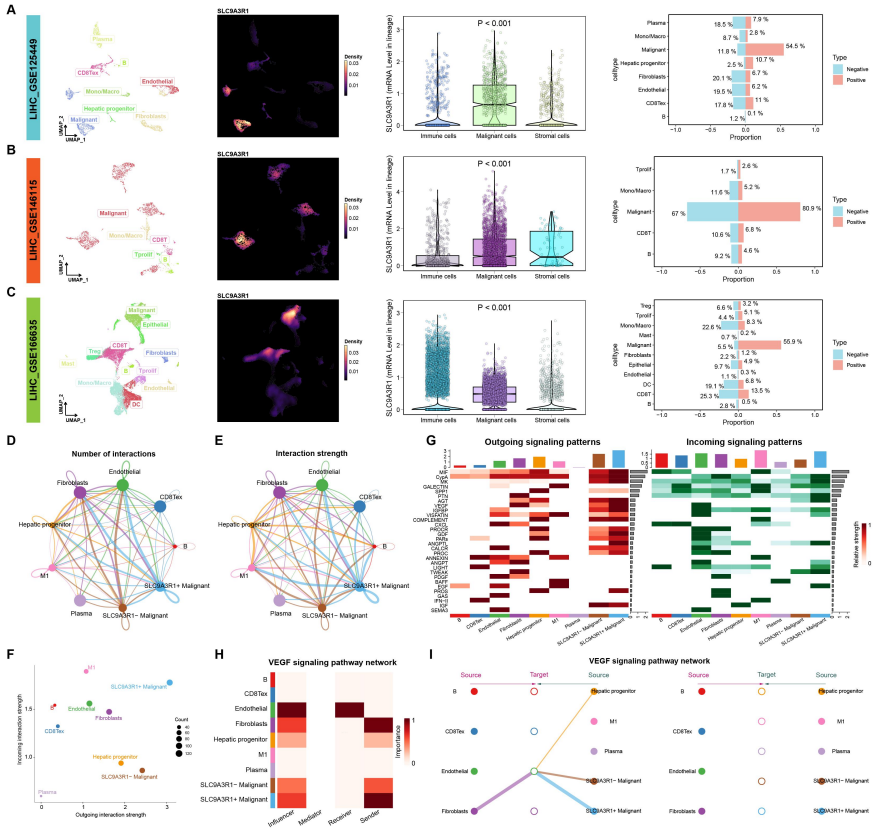

Figure 6. SLC9A3R1+ malignant cells act as signaling hubs coordinating the microenvironment through the VEGF pathway. (A-C). Single-cell transcriptomic landscape of HCC from three independent cohorts (GSE125449, GSE146115, GSE166635) visualized by UMAP dimensionality reduction; (D). Cellular interaction network analyzed by CellChat algorithm, demonstrating interaction numbers among different cell types in the TME; (E). Comparison of overall communication strength across different cell populations quantified by CellChat; (F). Signaling role analysis evaluating the outgoing and incoming communication patterns of different cell types in the TME; (G). Differential interaction analysis of VEGF signaling pathway between SLC9A3R1+ and SLC9A3R1- malignant cell populations; (H). VEGF signaling network architecture showing specific communication patterns between SLC9A3R1+ malignant cells and stromal components.

CNV, expression characteristics, and association with immune microenvironment and molecular subtypes of SLC9A3R1 in HCC

This study systematically investigated the CNVs, expression levels, and associations with the immune microenvironment and molecular subtypes of SLC9A3R1 in HCC. Figure 7A shows the distribution characteristics of genome-wide copy number variations in the TCGA-LIHC cohort (*n* = 370). The results indicate that all chromosomes in liver cancer tissues have varying degrees of copy number gains or losses, suggesting widespread genomic copy number instability in HCC. An integrated analysis revealed that elevated expression of SLC9A3R1 is significantly associated with increased genomic instability in HCC. The cohort with the highest expression levels (Q1) demonstrated a markedly increased global CNV burden, as indicated by FGA, FGG, and FGL metrics [Figure 7B]. Moreover, tumors with high SLC9A3R1 expression exhibited genome-wide increases in CNVs, characterized by distinct regional patterns: a significant enrichment of losses in tumor suppressor gene loci, such as 10q23.31-PTEN, and a heightened prevalence of gains in oncogene regions, including 17q25.3-BRIP1, 3q26.31-PIK3CA, and 2q24.1-SCN2A [Figure 7C]. To investigate the regulatory role of CNV in SLC9A3R1 on its expression, we examined the link between the genomic copy number of SLC9A3R1 and the corresponding mRNA expression metrics within the TCGA-LIHC dataset. The results demonstrated that SLC9A3R1 expression exhibited a stepwise increase with ascending copy number levels and showed a strong positive correlation with its copy number status ($R = 0.5$, $p = 5.97\times10^{-24}$). These findings clearly indicate that CNV serves as a key driver of SLC9A3R1 expression modulation [Figure 7D-E]. To thoroughly investigate the relationship between elevated SLC9A3R1 expression and genomic instability, an extensive examination was performed on the frequency and types of mutations in essential driver genes among the SLC9A3R1-high and SLC9A3R1-low expression cohorts in the TCGA-LIHC study. Our findings showed a notably increased mutation prevalence in the SLC9A3R1-High cohort in several tumor suppressor genes (TSGs) that are critically associated with genomic stability, including TP53 (23), FLG(24), SPTA1(25), and OBSCN(26), compared to the SLC9A3R1-Low group [Figure 7F]. At the same time, TMB and neoantigen burden were also significantly increased [Figure

7G-H]. Collectively, these results reveal that in HCC, high expression of SLC9A3R1 correlates with increased genomic instability and greater immunogenic potential. Examination of pathway enrichment demonstrated a clear link between SLC9A3R1 expression and heightened activity in signaling pathways connected to T cell receptors (TCR) and B cell receptors (BCR) (R = 0.21 and 0.35, $P = 4.1\times10^{-5}$ and 4.5×10^{-12}, respectively) [Figure 7I]. The distribution heterogeneity of its expression in HCC molecular subtypes is significant (high expression proportion in C4 subtype, low expression mainly in C3 subtype [Figure 7J]. Investigation of the immune microenvironment revealed that SLC9A3R1 expression exhibits a significant negative correlation with both immune cell priming and activation, as well as the overall infiltration of immune cells into the tumor during the cancer immune cycle. Conversely, recruitment of immunosuppressive entities, notably regulatory T cells (Treg), exhibited a positive correlation [Figure 7K]. To pinpoint the contribution of SLC9A3R1 to the tumor microenvironment, we leveraged a suite of immune infiltration algorithms to investigate the relationship between SLC9A3R1 expression levels and the immune landscape across ten distinct patient cohorts. The results indicated that SLC9A3R1 exhibited an overall negative correlation with immune cell infiltration. More importantly, immune scores, estimate scores and stromal scores were all negatively correlated, suggesting that SLC9A3R1 mediates tumor immune suppression [Figure 7L]. We further investigated the associations between SLC9A3R1 expression levels and diverse immunomodulatory genes, including components related to antigen presentation, immune stimulatory factors, chemokines, and chemokine receptors, across multiple HCC cohorts. The results indicated that SLC9A3R1 exhibited an overall negative correlation with these immune regulatory genes, a finding that is consistent with the aforementioned analysis conclusions [Figure 7M], further supporting the role of SLC9A3R1 in mediating tumor immune suppression within the microenvironment of HCC.

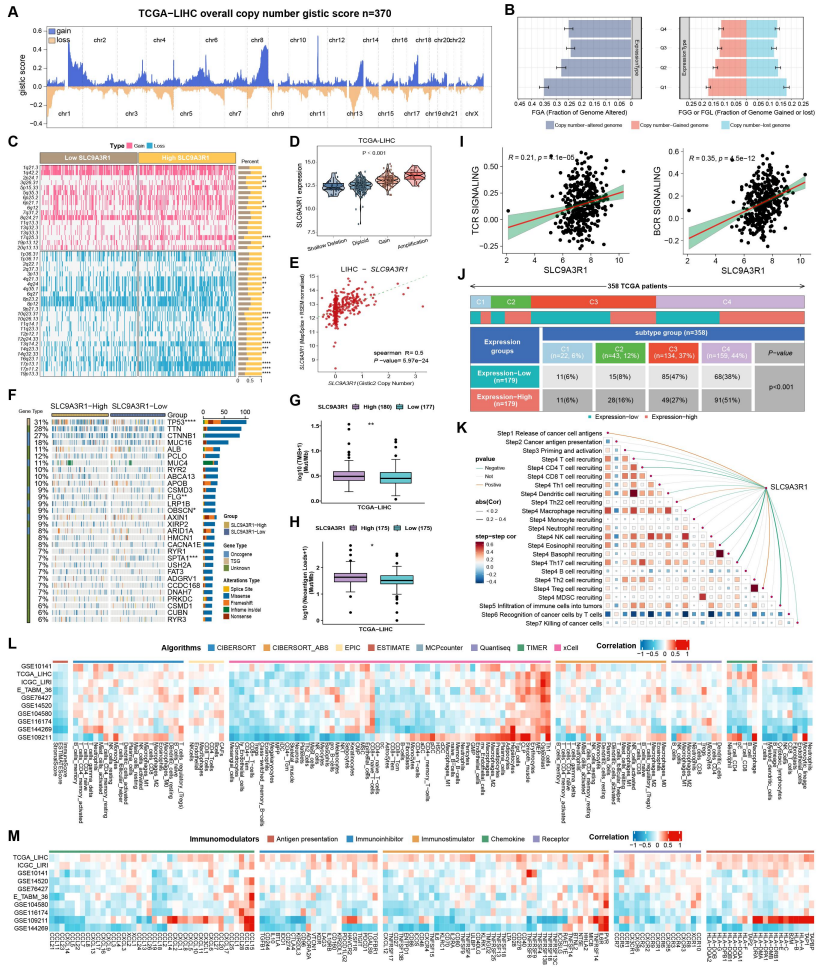

Figure 7. Copy number variation, expression characteristics, and association with immune microenvironment and molecular subtypes of SLC9A3R1 in HCC. (A). Genome-wide CNV gistic score profile of the TCGA-LIHC cohort (*n* = 370), displaying CNV alterations across chromosomes; (B-C) SLC9A3R1 CNV frequency (B) and CNV profile heatmap; (C). between its high and low-expression groups; (D-E) Correlation of SLC9A3R1 copy number with mRNA expression ($P < 0.001$) in LIHC; (F). Driver gene mutation profile (including TP53) in SLC9A3R1 high- *vs.* low-expression samples; (G-H). Boxplots of TMB (G) and neoantigen load (H) between SLC9A3R1 expression groups; (I). Correlation of SLC9A3R1 with TCR (R = 0.21, $P = 4.1 \times 10\text{-}5$) and BCR (R = 0.35, $P = 4.5 \times 10\text{-}12$) pathway activity; (J). Distribution of SLC9A3R1 expression groups across 4 HCC subtypes (C1-C4, $P <$ 0.001); (K). Correlation of SLC9A3R1 with cancer immunity cycle steps (TIP database); (L). Correlation of SLC9A3R1 with immune cells (multiple algorithms); (M).

Correlation of SLC9A3R1 with immunomodulatory molecules.

SLC9A3R1 regulates immune microenvironment components and modulates chemotherapy responses in HCC

The scatter plot analysis in Figure 8A revealed a significant negative correlation between SLC9A3R1 expression levels and tertiary lymphoid structure (TLS) score (R = -0.22, $P = 2.3 \times 10^{-5}$) in HCC. The box plot further validated that the TLS score was significantly lower in the high SLC9A3R1 expression group than in the low expression group. Evaluation of tumor immune escape [Figure 8B] revealed a notably higher Tumor Immune Dysfunction and Exclusion (TIDE) among patients with high SLC9A3R1 expression compared to those with low levels, suggesting a stronger immune escape potential. Further analysis of T cell functional characteristics revealed that SLC9A3R1 expression showed a significant negative correlation with T cell dysfunction level (R =- 0.314, $P = 2.26 \times 10^{-9}$), while demonstrating a significant positive correlation with T cell exclusion level (R = 0.306, $P = 5.86 \times 10^{-8}$) [Figure 8C-D]. These findings indicate that high SLC9A3R1 expression may play a role in creating an immunosuppressive environment in HCC, mainly by enhancing the exclusion of T cells. The heatmap analysis based on the CTRP database visually demonstrates the regulatory heterogeneity of SLC9A3R1 high expression in relation to the sensitivity/resistance of the top 20 chemotherapeutic agents across 10 different cohorts [Figure 8E]. A positive correlation between elevated expression levels and drug resistance is denoted in red (for instance, tyrosine kinase inhibitors such as canertinib and erlotinib), whereas blue signifies a positive correlation between high expression levels and drug sensitivity (for example, kinase inhibitors like YL54 and SCH-529074). Further IC50 analysis [Figures 8F-G] unveiled a significant correlation between the expression levels of SLC9A3R1 and the IC50 values for afatinib, indicating that increased SLC9A3R1 expression may enhance the resistance of HCC to afatinib. Conversely, SLC9A3R1 expression showed a significant negative correlation with the IC50 of SU11274, suggesting that its high expression may increase the therapeutic

sensitivity of HCC to SU11274. Based on the comprehensive analyses, SLC9A3R1 emerges as a key regulator that shapes the immunosuppressive TME, enhances sensitivity to immune checkpoint blockade therapy, and exhibits heterogeneous modulation of chemotherapeutic drug responses in HCC.

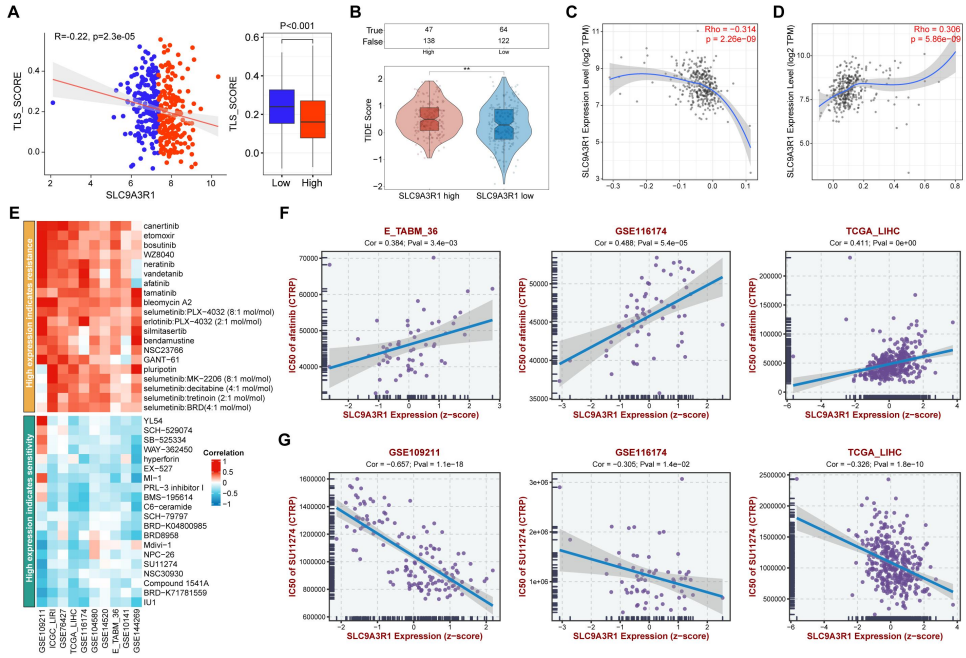

Figure 8. SLC9A3R1 regulates immune microenvironment components and modulates chemotherapy responses in HCC. (A). Scatter plot showing the correlation between SLC9A3R1 expression and tertiary lymphoid structure (TLS) score (R = -0.22, $P = 2.3 \times 10^{-5}$), with box plot comparing TLS scores between high and low SLC9A3R1 expression groups; (B) Box plot of TIDE in high *vs.* low SLC9A3R1 expression groups. (C-D) Relationship of SLC9A3R1 expression to T-cell dysfunction as shown in scatter plots (C: R = -0.314, $P = 2.26 \times 10^{-9}$) or T-cell exclusion level (D: R = 0.329, $P = 5.86 \times 10^{-8}$) from TIDE analysis; (E) Heatmap from CTRP database displaying the regulatory heterogeneity of high SLC9A3R1 expression on sensitivity/resistance to top 20 chemotherapeutic agents across 10 cohorts (red: positive correlation with resistance; blue: positive correlation with sensitivity); (F-G) Scatter plots of IC50 values for afatinib (F) and SU11274 (G) against SLC9A3R1 expression in HCC cohorts (GSE116174, TCGA-LIHC, *etc.*), with correlation coefficients and *P*-values.

Regulatory and enrichment analysis of SLC9A3R1 on HCC carcinogenic pathways, oncogenic phenotypes, and immune microenvironment

To elucidate the mechanistic role of SLC9A3R1 in the occurrence and development of liver cancer, we analyzed its expression and its correlation with the activity of eight classic oncogenic pathways (including NOTCH, HIPPO, HEDGEHOG, MAPK, MYC, TGF-β, WNT, and PI3K) based on the TCGA-LIHC cohort. The findings suggested a significant positive correlation between the activity of seven of these pathways and the expression levels of SLC9A3R1. Box plots further validated this trend—activity levels of all seven pathways in the high expression group of SLC9A3R1 were significantly higher than those in the low expression group [Figures 9A-H]. These findings suggest that SLC9A3R1 may synergistically promote the occurrence of liver cancer by positively regulating multiple oncogenic pathways, with a complex and pathway-specific regulatory role in liver cancer development. In the ICGC-LIHC-JP cohort, expression of SLC9A3R1 was positively correlated with all ten evaluated oncogenic phenotypes, including hypoxia (R = 0.27, $P = 3.0 \times 10^{-5}$), EMT (R = 0.22, $P = 0.018$), invasion ($R = 0.16$, $P = 0.017$), metastasis ($R = 0.31$, $P = 5.7 \times 10^{-4}$), proliferation (R = 0.36, $P = 4.2 \times 10^{-5}$), cell cycle (R = 0.41, $P = 5.7 \times 10^{-11}$), stemness (R = 0.23, $P = 3.6 \times 10^{-4}$), differentiation (R = 0.18, $P = 5.1 \times 10^{-3}$), DNA damage (R = 0.39, $P = 6.2 \times 10^{-10}$), and DNA repair (R = 0.45, $P = 9.5 \times 10^{-13}$) [Figure 9I]. These results provide strong evidence for SLC9A3R1 as a key driver in the pathogenesis of HCC, suggesting potential implications for therapeutic strategies targeting its downstream pathways. Enrichment analysis of tumor immune-related pathways revealed that SLC9A3R1 inhibits several signaling pathways in liver cancer, including the Cytokine-cytokine receptor interaction, Chemokine signaling pathway, Cytosolic DNA-sensing pathway, NOD-like receptor signaling pathway, and Lymphocyte chemotaxis. This suggests that its inhibition may lead to tumor cells escaping immune attack by blocking immune signal transduction and weakening the activation capacity of immune cells **[Figure 9J]**. The findings from the GSEA enrichment analysis

utilizing the Hallmark gene set suggest that, within the group with elevated expression of SLC9A3R1, there is a significant enrichment trend for core pro-cancer pathways related to tumor growth, proliferation, metabolism, and DNA repair (including Oxidative phosphorylation, E2F targets, G2m checkpoint, Myc targets v1, Mtorc1 signaling, DNA repair). In contrast, pathways associated with immune response, apoptosis, and the complement system (such as Apoptosis, Complement, Inflammatory response) show a significant downregulation in enrichment [Figure 9K]. This result is highly consistent with the phenotypic characteristics presented in Figures 9I-J.

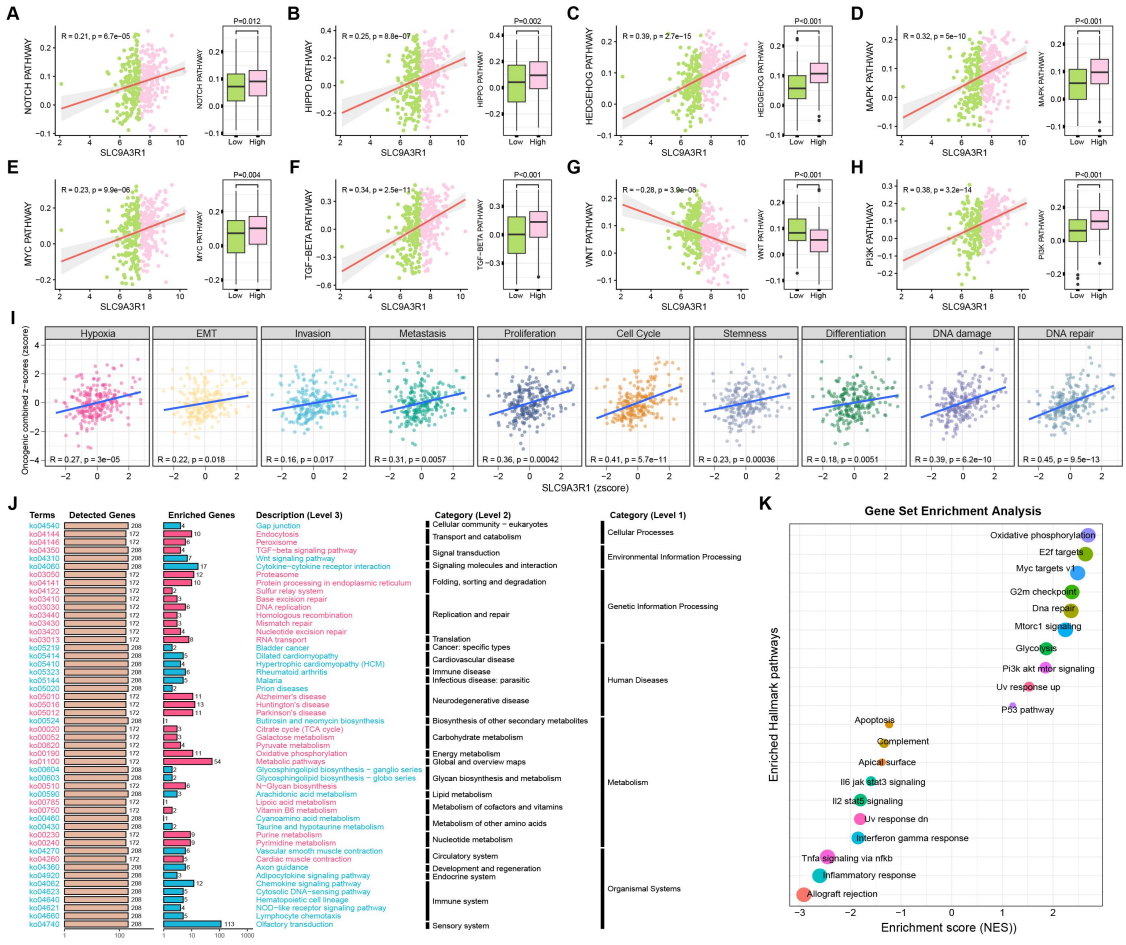

Figure 9. Association of SLC9A3R1 expression with oncogenic pathway activity, phenotypic traits, and immune-related pathway enrichment in liver cancer. (A-H) Scatter plots depicting correlations between SLC9A3R1 expression and activity of eight classic oncogenic pathways (NOTCH, HIPPO, HEDGEHOG, MAPK, MYC, TGF-β, WNT, PI3K) in the TCGA-LIHC cohort (with correlation coefficients and

P-values), plus box plots comparing pathway activity between high and low SLC9A3R1 expression groups; (I) Scatter plots showing correlations between SLC9A3R1 expression and ten oncogenic phenotypes (hypoxia, EMT, invasion, metastasis, proliferation, cell cycle, stemness, differentiation, DNA damage, DNA repair) in the ICGC-LIHC-JP cohort, each with correlation coefficients and *P*-values; (J) Enrichment analysis of tumor immune-related pathways, listing enriched pathways (e.g., Cytokine-cytokine receptor interaction, Chemokine signaling pathway) with detected/enriched gene counts and categorical classification (Cellular Processes, Environmental Information Processing, *etc.*); (K) GSEA using Hallmark gene sets, highlighting pro-cancer pathways (Oxidative phosphorylation, E2F targets, G2m checkpoint, *etc.*) enriched in the SLC9A3R1 high-expression group and downregulated immune/apoptosis pathways (Apoptosis, Complement, Inflammatory response), with normalized enrichment scores (NES) and *P*-values.

SLC9A3R1 exerts an oncogenic role in Hep 3B cells by regulating proliferation, apoptosis, migration and invasion

To explore the regulatory mechanism of the SLC9A3R1 gene on the malignant phenotype of Hep 3B cells, this study employed a variety of functional experiments for systematic analysis. The results of CCK-8 assays indicated a significant enhancement in the cell proliferation activity within the SLC9A3R1 overexpression group when compared to the control group, observed after 48, 72, and 96 h of culture. In contrast, the gene silencing group exhibited a marked decrease in proliferation ability at 72 and 96 h [Figure 10A]. Clonal formation experiments confirmed that SLC9A3R1 overexpression greatly enhanced the colony formation capability of the cells, while gene knockout resulted in a substantial reduction in colony numbers [Figure 10B]. These results collectively indicate that this gene exerts a positive regulatory effect on cell proliferation. Additionally, the results from both Transwell and wound healing assays consistently confirmed that SLC9A3R1 drives the migratory and invasive properties of Hep 3B cells, with overexpression enhancing and silencing suppressing

these malignant behaviors [Figures 10C-D]. To further elucidate the role of SLC9A3R1 in the response of Hep 3B cells to afatinib, we evaluated cell viability and apoptosis following drug treatment. CCK-8 assays were conducted to assess the survival of Hep 3B cells in both SLC9A3R1 overexpression and vector control groups, exposed to varying concentrations of afatinib. As illustrated in Figure 10E, the cell survival rate exhibited a decline in a dose-dependent manner with increasing afatinib concentrations in both groups, while SLC9A3R1 overexpression was found to diminish the sensitivity of Hep 3B cells to afatinib. Subsequently, flow cytometry was utilized to analyze apoptosis in the two groups post-afatinib treatment. Figure 10F demonstrates that the proportion of apoptotic cells was significantly lower in the SLC9A3R1 overexpression group compared to the vector control group. Overall, SLC9A3R1 fuels the aggressive cancerous behavior of Hep 3B cells by positively regulating cell proliferation, migration, and invasion abilities, while reducing their sensitivity to the drug afatinib.

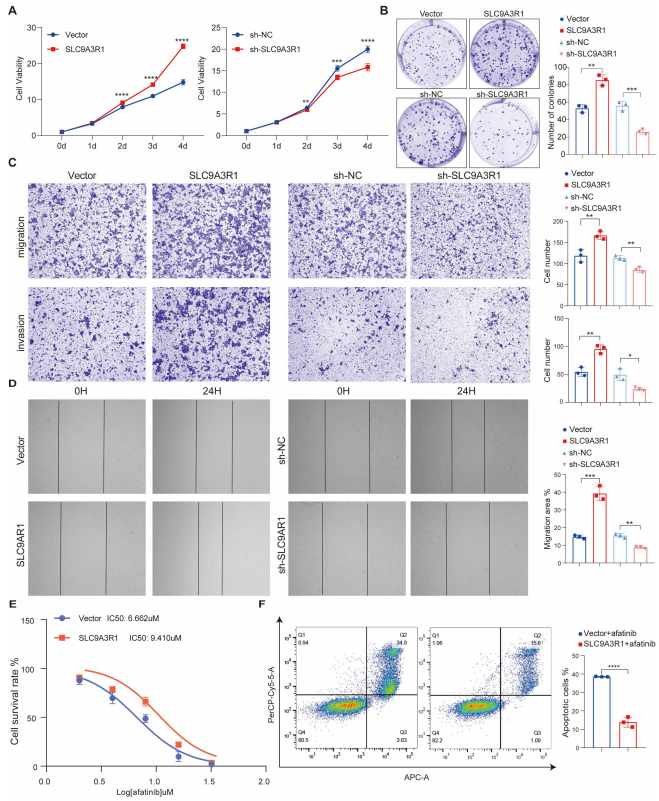

Figure 10. SLC9A3R1 exerts an oncogenic role in Hep3B cells by regulating proliferation, apoptosis, migration and invasion. (A). The CCK-8 assay assesses cell

proliferation rates in Hep 3B cells across 48, 72, and 96-h periods following either the overexpression (OE) or knockdown (KD) of SLC9A3R1; (B). The ability of Hep 3B cells to form colonies was examined in the context of SLC9A3R1 overexpression or knockdown; (C). Transwell assays evaluated migration and invasion in Hep 3B cells via SLC9A3R1 overexpression or knockdown; (D). Migration capacity of Hep 3B cells with modulated SLC9A3R1 expression was evaluated through wound healing assays; (E). The CCK-8 assay was utilized to gauge the viability of Hep 3B cells engineered to either carry a Vector control or overexpress SLC9A3R1, following exposure to varying doses of afatinib; (F). Apoptosis was analyzed via flow cytometry in Hep 3B cells-engineered for either SLC9A3R1 overexpression or knockdown-following treatment with serial concentrations of afatinib.

DISCUSSION

Precision diagnosis and treatment of HCC has always been a significant challenge in clinical practice, and identifying reliable molecular biomarkers is key to overcoming this bottleneck. This study systematically reveals the important role of SLC9A3R1, for the first time, from a pan-cancer perspective to a HCC-specific perspective, providing a solid theoretical basis for its clinical translation.

The systematic discoveries from pan-cancer analysis provide a significant foundation for liver cancer research. Our study demonstrates that SLC9A3R1 exhibits a markedly upregulated expression profile across various cancers[27,28], particularly prominent in BRCA[29], MM, and HCC[30]. This finding holds significance, it establishes SLC9A3R1 as an important molecule across cancer types, potentially involved in common pathways of tumorigenesis. Notably, CRISPR screening data indicate that SLC9A3R1 plays an indispensable role in specific tumor types such as leukemia, lymphoma, bladder cancer, and liver cancer. This cancer type-specific genetic dependency suggests that it may play a complex and diverse role in tumor biology. From the perspective of molecular mechanisms, SLC9A3R1 exhibits multi-layered characteristics. Its unique

subcellular localization pattern—dual distribution at the cell membrane and centrosome satellite region[10,31,32], along with spatial co-localization with the endoplasmic reticulum and microtubule network—supports the hypothesis of its function as a 'signal hub anchoring protein'. This localization feature enables it to integrate multiple key signaling pathways, coordinating cytoskeletal rearrangement and signal transduction. Additionally, cell cycle-specific expression analysis shows that SLC9A3R1 is significantly overexpressed during the G1 phase, a finding that aligns with its potential role in cell cycle regulation. Epigenetic analysis further reveals that its promoter region exhibits differential methylation patterns across various cancer types, which may partially explain the heterogeneity of its expression patterns across different cancers.

In the specific analysis of HCC, our findings hold greater clinical significance. The high expression of SLC9A3R1 in liver cancer tissues has been validated across multiple independent cohorts, demonstrating a high degree of consistency from transcriptomic to protein levels. Notably, its dynamic expression pattern during the progression of liver disease—showing a gradual upregulation from chronic hepatitis, cirrhosis to HCC—is particularly striking, with expression levels in advanced liver cancer significantly higher than those in early stages. This characteristic endows it with the capability to serve as a biomarker for tracking the progression of liver cancer. Furthermore, multicenter cohort analyses consistently corroborate that elevated levels of SLC9A3R1 are significantly linked to a worse prognosis in patients[33-35], and its value as an independent prognostic factor has been validated across different datasets.

The study highlights a compelling link between SLC9A3R1 expression and the tumor immune microenvironment, revealing that high levels of this protein are strongly correlated with an immunosuppressive landscape. This finding reveals a new mechanism by which SLC9A3R1 promotes tumor progression from an immunological perspective. Specifically, tumor regions with high SLC9A3R1 expression exhibited marked changes in immune cell infiltration patterns, including a decrease in the

proportion of effector T cells and an increase in immunosuppressive cell populations. These microenvironmental characteristics provide favorable conditions for tumor immune evasion[36-39]. Secondly, in terms of responses to chemotherapy and targeted therapy, SLC9A3R1 exhibits significant regulatory heterogeneity. Notably, its expression level shows an inverse correlation with the sensitivity to different drugs. For example, elevated levels of SLC9A3R1 show a strong positive correlation with increased IC50 values of Afatinib, which is an inhibitor of EGFR and HER2[40], suggesting a potential contribution to resistance to this drug. In contrast, its high expression is negatively correlated with the IC50 of SU11274 (a c-Met inhibitor)[41], indicating a potential enhancement of the sensitivity of tumor cells to this drug. In other words, SLC9A3R1 is not merely a factor of resistance or sensitization; rather, it differentially regulates drug response pathways by affecting specific downstream signaling networks. The roots of the heterogeneity in treatment responses are likely deeply rooted in the extensive regulation of core oncogenic pathways by SLC9A3R1. Our pathway activity analysis indicates that high expression of SLC9A3R1 is significantly positively correlated with the activation of multiple key oncogenic signaling pathways. This state of multi-pathway synergistic activation not only directly drives malignant phenotypes such as cell cycle progression, proliferation, EMT, and stem cell characteristics but may also fundamentally contribute to the complexity of drug responses. For instance, resistance to afatinib may be related to SLC9A3R1 maintaining or activating EGFR-independent alternative survival pathways (such as the aforementioned PI3K or MAPK pathways)[42]. In contrast, the sensitization to SU11274 may stem from a certain synergy or dependency between SLC9A3R1 and the c-Met pathway, making the inhibition of c-Met more detrimental to cells with high SLC9A3R1 expression[43]. In light of the established association of SLC9A3R1 with the activation of multiple oncogenic signaling pathways and potential resistance to afatinib, the detection of SLC9A3R1 expression can inform clinical decision-making: for patients with unsatisfactory efficacy of afatinib monotherapy, SLC9A3R1 test results can guide clinicians to avoid afatinib administration, or adopt a combination

regimen with PI3K or MAPK pathway inhibitors to overcome afatinib resistance. Meanwhile, the sensitization effect of SLC9A3R1 on SU11274 indicates that c-Met inhibitors may serve as a promising therapeutic option for patients with high SLC9A3R1 expression, which warrants stratified validation in well-designed clinical trials. Although this study reveals a potential association between SLC9A3R1 expression and clinical staging through the analysis of multiple public datasets, there are also some limitations. Firstly, there are platform differences and batch effects among the GEO cohorts relied upon in this study, and the sample sizes of some subgroups are limited, which may lead to insufficient statistical power and affect the generalizability of the results. Secondly, the standardization and completeness of clinical information across the datasets are inconsistent; for example, the absence of key covariates such as treatment regimens and follow-up times makes it difficult for us to fully control for potential confounding factors. Furthermore, this study is limited to bioinformatics analysis at the transcriptomic level and has not validated the specific biological mechanisms of SLC9A3R1 through functional experiments. Additionally, there is a lack of integrative support from multi-omics data such as genomics and proteomics, thus the interpretation of the role of this gene in disease remains preliminary. Future prospective studies and experimental validations are needed to further clarify its clinical and biological significance.

In conclusion, this study provides a systematic analysis from pan-cancer to HCC, establishing SLC9A3R1 as an important oncogene and revealing its specific role and clinical value in HCC. These results present fresh perspectives on the pathogenesis of liver cancer and provide potential molecular targets for the precise diagnosis and treatment of HCC. Future research should focus on exploring therapeutic strategies targeting SLC9A3R1 and advancing its translation into clinical applications.

CONCLUSION

Our comprehensive multi-omics analysis establishes SLC9A3R1 as a critical oncogenic

driver in HCC. The overexpression of SLC9A3R1, primarily resulting from copy number amplification, shows a strong correlation with increased genomic instability, signified by a heightened tumor mutation burden and notable changes in vital tumor suppressor genes. In functional terms, SLC9A3R1 promotes several pro-tumorigenic signaling pathways-such as NOTCH, HIPPO, and PI3K-while simultaneously creating an immunosuppressive TME, which features decreased T-cell infiltration and heightened immune exclusion. Additionally, SLC9A3R1 demonstrates varied effects on the sensitivity to a range of chemotherapeutic agents, further emphasizing its significance in tailored treatment approaches. Overall, these insights establish SLC9A3R1 as a promising prognostic marker, a predictive biomarker for immunotherapy responsiveness, and a potential target for therapy in HCC. Future research should aim to confirm these results in upcoming clinical studies and to clarify the intricate molecular mechanisms by which SLC9A3R1 orchestrates these complex oncogenic processes.

DECLARATIONS

Acknowledgments

We are grateful to the database for providing data support and to the editor and reviewers for their valuable comments.

Authors' contributions

Conceptualization, Writing-original draft, Formal Analysis: Y.W;
Resources, Software, Validation, Visualization: L.G;
Validation, Visualization: Q.L;
Formal Analysis, Investigation: C.W;
Validation, Visualization, Writing-original draft: Z.S;
Supervision, Visualization, Writing-review & editing: C.S.

Availability of data and materials

The data supporting this research is publicly available through various online archives.

The specific repository names and associated accession identifiers are listed within the manuscript or the Supplementary Material.

AI and AI-assisted Tools Statement

Not applicable.

Financial support and sponsorship

This work was supported by the Shandong Provincial Natural Science Foundation (ZR2022MH100).

Conflicts of interest

All authors declared that there are no conflicts of interest.

Ethical approval and consent to participate

Not applicable.

Consent for publication

Not applicable.

REFERENCES

1. Collaborators GBDCRF. The global burden of cancer attributable to risk factors, 2010-19: a systematic analysis for the Global Burden of Disease Study 2019. *Lancet.* 2022;400(10352):563-91.[PMID: 35988567 PMCID: PMC9395583 DOI: 10.1016/S0140-6736(22)01438-6]

2. Bray F, Laversanne M, Sung H, Ferlay J, Siegel RL, Soerjomataram I, et al. Global cancer statistics 2022: GLOBOCAN estimates of incidence and mortality worldwide

for 36 cancers in 185 countries. *CA Cancer J Clin.* 2024;74(3):229-63.[PMID: 38572751 DOI: 10.3322/caac.21834]

3. Lin CL, Kao JH. Development of hepatocellular carcinoma in treated and untreated patients with chronic hepatitis B virus infection. *Clin Mol Hepatol.* 2023;29(3):605-22.[PMID: 36788759 PMCID: PMC10366811 DOI: 10.3350/cmh.2022.0342]

4. Shen J, Qi W, Dai J, Leng S, Jiang K, Zhang Y, et al. Tenofovir vs. entecavir on recurrence of hepatitis B virus-related hepatocellular carcinoma beyond Milan criteria after hepatectomy. *Chin Med J (Engl).* 2021;135(3):301-8.[PMID: 34958539 PMCID: PMC8812695 DOI: 10.1097/CM9.0000000000001864]

5. Chen M, Li J, Shu G, Shen L, Qiao E, Zhang N, et al. Homogenous multifunctional microspheres induce ferroptosis to promote the anti-hepatocarcinoma effect of chemoembolization. *J Nanobiotechnology.* 2022;20(1):179.[PMID: 35366904 PMCID: PMC8976998 DOI: 10.1186/s12951-022-01385-x]

6. Sun J, Zhou C, Zhao Y, et al., Quiescin sulfhydryl oxidase 1 promotes sorafenib-induced ferroptosis in hepatocellular carcinoma by driving EGFR endosomal trafficking and inhibiting NRF2 activation. *Redox Biol.* 2021;41:101942.[PMID: 33770521 PMCID: PMC8024711 DOI: 10.1016/j.redox.2021.101942]

7. Villanueva A. Hepatocellular Carcinoma. *N Engl J Med.* 2019;380(15):1450-62.[PMID: 30970190 DOI: 10.1056/NEJMra1713263]

8. Liu H, Ma Y, He HW, Wang JP, Jiang JD, Shao RG. SLC9A3R1 stimulates autophagy via BECN1 stabilization in breast cancer cells. *Autophagy.* 2015;11(12):2323-34.[PMID: 26218645 PMCID: PMC4835148 DOI: 10.1080/15548627.2015.1074372]

9. Oh YS, Heo K, Kim EK, et al., Dynamic relocalization of NHERF1 mediates chemotactic migration of ovarian cancer cells toward lysophosphatidic acid stimulation. *Exp Mol Med.* 2017;49(7):e351.[PMID: 28684865 PMCID: PMC5565956 DOI: 10.1038/emm.2017.88]

10. Vaquero J, Nguyen Ho-Bouldoires TH, Claperon A, Fouassier L. Role of the PDZ-scaffold protein NHERF1/EBP50 in cancer biology: from signaling regulation to clinical relevance. *Oncogene.* 2017;36(22):3067-79.[PMID: 28068322 DOI: 10.1038/onc.2016.462]

11. Georgescu MM, Gagea M, Cote G. NHERF1/EBP_{50} Suppresses Wnt-beta-Catenin Pathway-Driven Intestinal Neoplasia. *Neoplasia.* 2016;18(8):512-23.[PMID: 27566107 PMCID: PMC5018097 DOI: 10.1016/j.neo.2016.07.003]

12. Saponaro C, Sergio S, Coluccia A, et al., β-catenin knockdown promotes NHERF1-mediated survival of colorectal cancer cells: implications for a double-targeted therapy. *Oncogene.* 2018;37(24):3301-16.[PMID: 29551770 PMCID: PMC6002344 DOI: 10.1038/s41388-018-0170-y]

13. Itou T, Ishibashi Y, Oguri Y, et al., EBP50 Depletion and Nuclear beta-Catenin Accumulation Engender Aggressive Behavior of Colorectal Carcinoma through Induction of Tumor Budding. *Cancers (Basel).* 2023;16(1).[PMID: 38201610 PMCID: PMC10778391 DOI: 10.3390/cancers16010183]

14. Jeong J, Yoo K, Lee J, Shin JH, Choi J, Wysolmerski J. Erbin interacts with NHERF1 and Ezrin to stabilize a membrane ErbB2 signaling complex in HER2-positive breast cancer. *Breast Cancer Res.* 2025;27(1):85.[PMID: 40390040 PMCID: PMC12090624 DOI: 10.1186/s13058-025-02025-6]

15. Schirosi L, Saponaro C, Giotta F, et al., Tumor Infiltrating Lymphocytes and NHERF1 Impact on Prognosis of Breast Cancer Patients. *Transl Oncol.* 2020;13(2):186-92.[PMID: 31865181 PMCID: PMC6931214 DOI: 10.1016/j.tranon.2019.10.020]

16. Mehtar A, Wechsler J, Desterke C, et al., Optimizing Detection of Circulating Tumor Cells in Breast Cancer: Unveiling New Markers for Clinical Applications. *Int J Mol Sci.* 2025;26(10).[PMID: 40429857 PMCID: PMC12111556 DOI: 10.3390/ijms26104714]

17. Jordaens S, Oeyen E, Willems H, et al., Protein Biomarker Discovery Studies on Urinary sEV Fractions Separated with UF-SEC for the First Diagnosis and Detection of

Recurrence in Bladder Cancer Patients. *Biomolecules.* 2023;13(6).[PMID: 37371512 PMCID: PMC10296596 DOI: 10.3390/biom13060932]

18. Thul PJ, Akesson L, Wiking M, et al., A subcellular map of the human proteome. *Science.* 2017;356(6340).[PMID: 28495876 DOI: 10.1126/science.aal3321]

19. Lee JS, Ruppin E. Multiomics Prediction of Response Rates to Therapies to Inhibit Programmed Cell Death 1 and Programmed Cell Death 1 Ligand 1. *JAMA Oncol.* 2019;5(11):1614-8.[PMID: 31436822 PMCID: PMC6707018 DOI: 10.1001/jamaoncol.2019.2311]

20. Thorsson V, Gibbs DL, Brown SD, et al., The Immune Landscape of Cancer. *Immunity.* 2018;48(4):812-30 e14.[PMID: 29628290 PMCID: PMC5982584 DOI: 10.1016/j.immuni.2018.03.023]

21. Liu Y, Xun Z, Ma K, et al., Identification of a tumour immune barrier in the HCC microenvironment that determines the efficacy of immunotherapy. *J Hepatol.* 2023;78(4):770-82.[PMID: 36708811 DOI: 10.1016/j.jhep.2023.01.011]

22. Wu R, Guo W, Qiu X, et al., Comprehensive analysis of spatial architecture in primary liver cancer. *Sci Adv.* 2021;7(51):eabg3750.[PMID: 34919432 PMCID: PMC8683021 DOI: 10.1126/sciadv.abg3750]

23. Levine AJ. p53: 800 million years of evolution and 40 years of discovery. *Nat Rev Cancer.* 2020;20(8):471-80.[PMID: 32404993 DOI: 10.1038/s41568-020-0262-1]

24. Yicheng F, Xin L, Tian Y, Huilin L. Association of *FLG* mutation with tumor mutation load and clinical outcomes in patients with gastric cancer. *Front Genet.* 2022;13:808542.[PMID: 36046250 PMCID: PMC9421250 DOI: 10.3389/fgene.2022.808542]

25. Yao J, You Q, Zhang X, et al., PIK3CA somatic mutations as potential biomarker for immunotherapy in elder or TP53 mutated gastric cancer patients. *Clin Genet.* 2023;103(2):200-8.[PMID: 36346122 DOI: 10.1111/cge.14260]

26. Bokor BA, Abdolreza A, Pal M, Battyani Z, Szell M, Nagy N. A Novel Germline Frameshift Variant in the Tumor Suppressor Gene OBSCN in a Melanoma Patient. *Int J*

Mol Sci. 2025;26(21).[PMID: 41226589 PMCID: PMC12609535 DOI: 10.3390/ijms262110553]

27. Georgescu MM, Mobley BC, Orr BA, et al., NHERF1/EBP50 and NF2 as diagnostic markers for choroid plexus tumors. *Acta Neuropathol Commun.* 2016;4(1):55.[PMID: 27229317 PMCID: PMC4882843 DOI: 10.1186/s40478-016-0329-0]

28. Bushau-Sprinkle AM, Lederer ED. New roles of the Na(+)/H(+) exchange regulatory factor 1 scaffolding protein: a review. *Am J Physiol Renal Physiol.* 2020;318(3):F804-8.[PMID: 31984791 PMCID: PMC7395471 DOI: 10.1152/ajprenal.00467.2019]

29. Sonnessa M, Sergio S, Saponaro C, et al., The Biological Relevance of NHERF1 Protein in Gynecological Tumors. *Front Oncol.* 2022;12:836630.[PMID: 35223518 PMCID: PMC8878902 DOI: 10.3389/fonc.2022.836630]

30. Shibata T, Chuma M, Kokubu A, Sakamoto M, Hirohashi S. EBP50, a beta-catenin-associating protein, enhances Wnt signaling and is over-expressed in hepatocellular carcinoma. *Hepatology*. 2003;38(1):178-86.[PMID: 12830000 DOI: 10.1053/jhep.2003.50270

31. Aksionau A, Silva RA, Hartman B, Flowers A. NHERF1/EBP50 immunoexpression in renal cell carcinomas and oncocytomas with ultrastructural analysis of clear cell renal cell carcinoma. *Transl Androl Urol.* 2023;12(8):1283-95.[PMID: 37680228 PMCID: PMC10481195 DOI: 10.21037/tau-23-101]

32. Bretscher A, Chambers D, Nguyen R, Reczek D. ERM-Merlin and EBP50 protein families in plasma membrane organization and function. *Annu Rev Cell Dev Biol.* 2000;16:113-43.[PMID: 11031232 DOI: 10.1146/annurev.cellbio.16.1.113

33. Nakagawa M, Matsumoto T, Yokoi A, et al., Interaction between membranous EBP50 and myosin 9 as a favorable prognostic factor in ovarian clear cell carcinoma. *Mol Oncol.* 2023;17(10):2168-82.[PMID: 37539980 PMCID: PMC10552901 DOI: 10.1002/1878-0261.13503]

34. Leiphrakpam PD, Lazenby AJ, Chowdhury S, et al., Prognostic and therapeutic implications of NHERF1 expression and regulation in colorectal cancer. *J Surg Oncol.* 2020;121(3):547-60.[PMID: 31867736 PMCID: PMC6996851 DOI: 10.1002/jso.25805]

35. Saponaro C, Malfettone A, Dell'Endice TS, et al., The prognostic value of the Na(+)/ H(+) exchanger regulatory factor 1 (NHERF1) protein in cancer. *Cancer Biomark.* 2014;14(2-3):177-84.[PMID: 24878819 PMCID: PMC12928374 DOI: 10.3233/CBM-130329]

36. Saponaro C, Vagheggini A, Scarpi E, et al., NHERF1 and tumor microenvironment: a new scene in invasive breast carcinoma. *J Exp Clin Cancer Res.* 2018;37(1):96.[PMID: 29716631 PMCID: PMC5930748 DOI: 10.1186/s13046-018-0766-7]

37. Malfettone A, Silvestris N, Paradiso A, Mattioli E, Simone G, Mangia A. Overexpression of nuclear NHERF1 in advanced colorectal cancer: association with hypoxic microenvironment and tumor invasive phenotype. *Exp Mol Pathol.* 2012;92(3):296-303.[PMID: 22440733 DOI: 10.1016/j.yexmp.2012.03.004]

38. Salie H, Wischer L, D'Alessio A, et al., Spatial single-cell profiling and neighbourhood analysis reveal the determinants of immune architecture connected to checkpoint inhibitor therapy outcome in hepatocellular carcinoma. *Gut.* 2025;74(3):451-66.[PMID: 39349005 PMCID: PMC11874287 DOI: 10.1136/gutjnl-2024-332837]

39. Wang L, Geng H, Liu Y, et al., Hot and cold tumors: Immunological features and the therapeutic strategies. *MedComm (2020).* 2023;4(5):e343.[PMID: 37638340 PMCID: PMC10458686 DOI: 10.1002/mco2.343]

40. Zhou Y, Yu L, Huang P, et al., Identification of afatinib-associated ADH1B and potential small-molecule drugs targeting ADH1B for hepatocellular carcinoma. *Front Pharmacol.* 2023;14:1166454.[PMID: 37229243 PMCID: PMC10203513 DOI: 10.3389/fphar.2023.1166454]

41. Inagaki Y, Qi F, Gao J, Qu X, et al., Effect of c-Met inhibitor SU11274 on hepatocellular carcinoma cell growth. *Biosci Trends.* 2011;5(2):52-6.[PMID: 21572247 DOI: 10.5582/bst.2011.v5.2.52]

42. Coco S, Truini A, Alama A, et al., Afatinib resistance in non-small cell lung cancer involves the PI3K/AKT and MAPK/ERK signalling pathways and epithelial-to-mesenchymal transition. *Target Oncol.* 2015;10(3):393-404.[PMID: 25341405 DOI: 10.1007/s11523-014-0344-7]

43. Yu Y, Peng XD, Qian XJ, et al., Fis1 phosphorylation by Met promotes mitochondrial fission and hepatocellular carcinoma metastasis. *Signal Transduct Target Ther.* 2021;6(1):401.[PMID: 34848680 PMCID: PMC8632923 DOI: 10.1038/s41392-021-00790-2]